The Projector-Augmented Plane Wave Method Applied to Molecular Bonding

M. Valiev and J. H. Weare*

Department of Chemistry, University of California, San Diego, La Jolla, California 92093-0340

Received: August 23, 1999; In Final Form: October 11, 1999

The projector-augmented wave (PAW) method proposed by Blöchl is an all-electron ab initio approach to electronic structure calculations. Using a local basis set expansion, the LSDA wave function is mapped onto a smooth image which can be treated with a plane wave basis set of a practical size. We discuss our implementation of this approach and its application to the calculation of the bonding properties of several second row and transition metal diatomic molecules. Comparisons are made between PAW and other methods. Our results for binding energy, bond length, and vibration frequency indicate that the accuracy of the PAW method is similar to that of local basis and finite grid methods. The convergence with respect to number of plane waves is sufficient that practical calculations are possible even for systems which would be difficult to treat with pseudopotential methods. For example, for the F_2 and Fe_2 dimers the bonding energy is converged with a 60 Ry cutoff in the plane wave expansion. The local basis contributions that appear in the theory can be precomputed, and therefore, the overhead typically associated with the local basis method is greatly reduced. For a fixed size of the plane wave basis set the execution times of the PAW method are similar to those of plane wave pseudopotential methods.

1. Introduction

Ab initio electronic structure calculations in material science are making increasingly important contributions to the interpretation of experimental data and are providing new insights into processes which are otherwise inaccessible to laboratory probes. Generally material problems are sufficiently complicated that the preferred method of electronic structure calculation is based on density-functional theory (DFT) within the local spin density approximation (LSDA).[11] The central quantity in this method is the energy functional $E[\{\Psi_n\}]$, which for a typical molecular system is given by

$$E[\{\Psi_n\}] = T + W + E_{xc} \tag{1.1}$$

where T is a kinetic energy,

$$T = \sum_n f_n \left\langle \Psi_n \left| -\frac{1}{2}\nabla^2 \right| \Psi_n \right\rangle \tag{1.2}$$

W denotes the Hartree energy,

$$W = \frac{1}{2}\int\int \frac{(n(\mathbf{r}) + n_c(\mathbf{r}) - n_Z(\mathbf{r}))(n(\mathbf{r}') + n_c(\mathbf{r}') - n_Z(\mathbf{r}'))}{|\mathbf{r} - \mathbf{r}'|} d\mathbf{r} d\mathbf{r}' \tag{1.3}$$

E_{xc} is the exchange−correlation energy,

$$E_{xc} = \int \epsilon_{xc}(n(\mathbf{r}) + n_c(\mathbf{r}))(n(\mathbf{r}) + n_c(\mathbf{r}))d\mathbf{r} \tag{1.4}$$

Here $\{\Psi_n\}$ represent a set of auxiliary single particle orbitals, also known as Kohn−Sham orbitals. The valence density $n(\mathbf{r})$ is defined as

$$n(\mathbf{r}) = \sum_n f_n |\Psi_n(\mathbf{r})|^2$$

The density $n_c(\mathbf{r}) = \sum_a n_c^a(\mathbf{r} - \mathbf{R}^a)$ is the sum of the core charge densities, and $n_Z(\mathbf{r}) = \sum_a Z^a \delta(\mathbf{r} - \mathbf{R}^a)$ represents the sum of the ion charge densities over the atomic sites a. Although not indicated explicitly, the constant infinite ion self energy term in (1.3) is assumed to be subtracted out. The total energy and the density of the ground state can be found by minimizing $E[\{\Psi_n\}]$ with respect to $\Psi_n(\mathbf{r})$, subject to orthogonality constraints. This leads to the effective Schrödinger equation:

$$H|\Psi_i\rangle = \epsilon_i|\Psi_i\rangle, \quad (i = 1, ..., N) \tag{1.5}$$

where Hamiltonian H is given by

$$H(\mathbf{r}) = -\frac{1}{2}\nabla^2 + \int \frac{n(\mathbf{r}') + n_c(\mathbf{r}') - n_Z(\mathbf{r}')}{|\mathbf{r} - \mathbf{r}'|} d\mathbf{r}' + v_{xc}(\mathbf{r}) \tag{1.6}$$

Here, $v_{xc}(r)$ represents the exchange−correlation potential:

$$v_{xc}(\mathbf{r}) = \frac{\delta E_{xc}}{\delta n(\mathbf{r})} \tag{1.7}$$

Since the exchange−correlation potential is a function of the electron density, the single-electron equations (1.5) are coupled and require a self-consistent solution. In practice, the solution of (1.5) proceeds by expanding $\Psi_n(\mathbf{r})$ in terms of a predetermined finite set of basis functions $\{\chi_\alpha(\mathbf{r})\}$

$$\Psi_n(\mathbf{r}) = \sum_\alpha c_{n,\alpha}\chi_\alpha(\mathbf{r}) \tag{1.8}$$

The traditional choice for $\{\chi_\alpha(\mathbf{r})\}$ in chemical applications is a set local basis functions centered around the atoms. Common examples are the numerical solutions to the corresponding atomic problems[10] or various Gaussian functions.[9] The local basis approach provides an efficient expansion of the wave

10.1021/jp9929770 CCC: $18.00
Published on Web 12/09/1999

function. However, it also requires evaluation of many multicenter integrals, which makes these methods difficult to apply to large systems even for a single geometric configuration. This prevents an efficient application of the local basis set methods in dynamical problems, such as chemical reactions in condensed phases, position optimization in large molecules, etc.

A different method of solution of the LSDA equations, in which the basis $\{\chi_\alpha(\mathbf{r})\}$ consists of the plane waves,

$$\chi_\alpha(\mathbf{r}) = \mathrm{e}^{-i\mathbf{k}_\alpha\mathbf{r}} \tag{1.9}$$

has been used in condensed matter physics. The main obstacle in this approach is that the accurate representation of the quickly varying valence wave functions in regions near the nucleus requires an impracticably large number of plane waves. The problem can be partially alleviated by the introduction of pseudopotentials,[19] where the deep Coulomb potential, the second term of the right of (1.6), is replaced by a shallow smooth norm-conserving pseudopotential. The pseudopotential reduces the number of nodes in the valence wave functions and relaxes the requirements on the size of the plane wave basis. The availability of fast Fourier transformations (FFT) algorithms and independence of the atomic positions in plane wave basis set methods proves to be major advantage in the dynamical problems. Ab initio molecular dynamics methods[20] (such as the Car−Parrinelo method[8]) allow a rapid update of the solution as the geometry of the system evolves.

The major limiting factor in plane wave methods remains the availability of smooth and transferable pseudopotentials. The generation of a smooth pseudopotential is especially problematic for the elements that possess strongly localized nodeless valence orbitals. These are, for example, 2p states in O, F, 3d states in transition metals, etc. Strictly speaking the replacement of the actual potential with the pseudopotential should only take place close to the nucleus. However, the small size of the replacement volume results in steep pseudopotential if norm conservation is retained.[23] In practice, one is often forced to "soften" the pseudopotential, i.e., extend it all the way into the bonding region and sometimes even into the neighboring atom. This compromises the transferability of the pseudopotential and can lead to undesired side effects. Finally, the introduction of the pseudopotential also results in the loss of the all-electron information which is necessary for some applications.

Having discussed pros and cons of the local and plane wave basis sets it is natural to conclude that a mixed basis set might offer the best possible approach to the solution of (1.5). This has been recognized for some time in computational solid state and a number methods have been developed.[19] Ideally, a mixed basis method should not require an introduction of the pseudopotential since the rapid variation of the valence orbitals can be described via local basis functions. On the other hand, it has to be efficient enough to allow an implementation in dynamical problems. An important breakthrough in this area has been made with the introduction of the projector-augmented wave method (PAW) by Blöchl.[7] In the center of this method is a transformation that maps the solutions to (1.5) to a smoother functions that can be expanded in plane waves. The rapidly varying remainders of the wave functions instead of being discarded as in pseudopotential methods are now treated with the help of the local basis set. Unlike the pure local basis methods, the evaluation of the multicenter integrals is avoided in PAW method. This allows for greater flexibility in treating orbitals with short length scales without the fear of losing relevant physical information and retains numerical efficiency. In this article we discuss the implementation of the PAW method and its applications to some systems (e.g., F_2, Fe_2, etc.) that are difficult to treat with norm-conserving pseudopotential methods. Our comparison of the results of this method to norm-conserving pseudopotential calculations and local basis set calculations indicates the following: (i) The accuracy of the PAW is similar to the accuracy of a local basis calculation. (ii) The convergence with respect to the plane wave basis set leads to practical calculations even for difficult systems (F, transition metals). (iii) The bonding properties in transition metals are described correctly for a wide range of bond distances, from diatomic molecules to solids.[12,15] (iv) The accuracy of the calculations can be systematically improved by expanding the local representation. (v) The method is robust with respect to the choice of the local basis set. (vi) Local basis set terms in the Hamiltonian are one center and can be precomputed so that execution times are similar to the plane wave pseudopotential methods.

2. Description of PAW Method

2.1. Transformation. Let us consider the Schrödinger equation (1.5) for a generic atomic cluster system. It can be observed that its solutions, the wave functions $\{\Psi_n\}$, share the common behavior: they rapidly oscillate in the neighborhood of the atomic nuclei and become fairly flat in the region between the atoms. This suggests the division of the whole space Ω in two distinct regions: the collection of *nonoverlapping* spherical regions around each atom: atomic spheres region $\cup_a\Omega_a$, and the remainder, the interstitial region Ω_I:

$$\Omega = \Omega_I + \cup_a\Omega_a$$

It is clear that the plane wave basis, being the ideal choice in the interstitial region Ω_I, will have great difficulties describing the wave function $\Psi_n(\mathbf{r})$ in the atomic spheres region $\cup_a\Omega_a$. In PAW method this problem is circumvented by introducing auxiliary wave function $\tilde{\Psi}_n(\mathbf{r})$, which satisfies the following requirements. First, $\tilde{\Psi}_n(\mathbf{r})$ can be obtained from $\Psi_n(\mathbf{r})$ via the invertible linear transformation Y

$$|\tilde{\Psi}_n\rangle = \mathrm{Y}|\Psi_n\rangle \tag{2.1}$$

$$|\Psi_n\rangle = \mathrm{Y}^{-1}|\tilde{\Psi}_n\rangle \tag{2.2}$$

Second, $\tilde{\Psi}_n(\mathbf{r})$ is smooth, i.e., can be represented by plane wave basis set of a practical size, everywhere, including the atomic spheres region,

$$\tilde{\Psi}_n(\mathbf{r}) = \sum_{|\mathbf{k}|<k_{\max}} c(\mathbf{k})\,\mathrm{e}^{-i\mathbf{k}\mathbf{r}} \tag{2.3}$$

The first requirement ensures that the task of solving Schrödinger equation (1.5) can be equivalently reformulated in terms of $\tilde{\Psi}_n(\mathbf{r})$, whereas the second requirement allows the entire process to be performed using the plane wave basis set.

The actual construction of $\tilde{\Psi}_n(\mathbf{r})$ from a given $\Psi_n(\mathbf{r})$ proceeds as follows. For each atom, we define a finite set of local basis functions $\{\phi_\alpha^a\}$ that is expected to accurately describe the oscillating behavior of the relevant wave function $\Psi_n(\mathbf{r})$ within the corresponding atomic sphere. Associated with $\{\phi_\alpha^a\}$ we introduce a set of localized projector functions $\{p_\alpha^a\}$ such that

$$\langle p_\beta^a|\phi_\alpha^a\rangle = \delta_{\alpha\beta} \tag{2.4}$$

$$p_\alpha^a(\mathbf{r}) = 0, \quad \forall\mathbf{r} \subset \Omega_I \tag{2.5}$$

Using $\{\phi_\alpha^a\}$ and $\{p_\alpha^a\}$, the wave function $\Psi_n(\mathbf{r})$ in the atomic sphere region can be represented as

$$\Psi_n(\mathbf{r}) = \sum_\alpha c_{n,\alpha}^a \phi_\alpha^a(\mathbf{r}) + \Delta_n^a(\mathbf{r}), \quad \forall \mathbf{r} \subset \Omega_a \tag{2.6}$$

The coefficients $c_{n,\alpha}^a$ in the expansion (2.6) are given by

$$c_{n,\alpha}^a = \langle p_\alpha^a | \Psi_n \rangle \tag{2.7}$$

The correction

$$|\Delta_n^a\rangle = (1 - \sum_\alpha |\phi_\alpha^a\rangle\langle p_\alpha^a|)|\Psi_n\rangle \tag{2.8}$$

reflects the incompleteness of set $\{\phi_\alpha^a\}$. As the size of the basis $\{\phi_\alpha^a\}$ gets larger, the local basis representation of $\Psi_n(\mathbf{r})$ (first term in (2.6)) becomes more accurate, and $\Delta_n^a(\mathbf{r})$ goes to zero. To define a mapping into $\tilde{\Psi}_n(\mathbf{r})$, we now form an auxiliary smooth basis set $\{\tilde{\phi}_\alpha^a\}$ subject to the following conditions. First, the basis function $\tilde{\phi}_\alpha^a(\mathbf{r})$ is smooth, i.e., expandable in terms of the plane wave basis of a practical size, everywhere including the atomic sphere region. Second, $\tilde{\phi}_\alpha^a(\mathbf{r})$ merges differentiably into $\phi_\alpha^a(\mathbf{r})$ outside the atomic sphere:

$$\tilde{\phi}_\alpha^a(\mathbf{r}) = \phi_\alpha^a(\mathbf{r}), \quad \forall \mathbf{r} \subset \Omega_I \tag{2.9}$$

Third, both $\tilde{\phi}_\alpha^a(\mathbf{r})$ and differences $\tilde{\phi}_\alpha^a(\mathbf{r}) - \phi_\alpha^a(\mathbf{r})$ form linearly independent sets. The smooth wave function $\tilde{\Psi}_n(\mathbf{r})$ can be obtained based on the following prescription. Inside the atomic sphere region it is generated by replacing each occurrence of $\phi_\alpha^a(\mathbf{r})$ with $\tilde{\phi}_\alpha^a(\mathbf{r})$ in the expansion (2.6)

$$\tilde{\Psi}_n(\mathbf{r}) = \sum_\alpha c_{n,\alpha}^a \phi_\alpha^a(\mathbf{r}) + \Delta_n^a(\mathbf{r}), \quad \forall \mathbf{r} \subset \Omega_a \tag{2.10}$$

whereas in the interstitial region it simply coincides with $\Psi_n(\mathbf{r})$:

$$\tilde{\Psi}_n(\mathbf{r}) = \Psi_n(\mathbf{r}), \quad \forall \mathbf{r} \subset \Omega_I$$

In more quantitative terms the transformation Y between $\Psi_n(\mathbf{r})$ and $\tilde{\Psi}_n(\mathbf{r})$ (see (2.1)) can be represented as

$$\mathrm{Y} = 1 + \sum_a \sum_\alpha (|\tilde{\phi}_\alpha^a\rangle - |\phi_\alpha^a\rangle)\langle p_\alpha^a| \tag{2.11}$$

Its inverse can be obtained as

$$\mathrm{Y}^{-1} = 1 + \sum_a \sum_\alpha (|\phi_\alpha^a\rangle - |\tilde{\phi}_\alpha^a\rangle)\langle \tilde{p}_\alpha^a| \tag{2.12}$$

where a set of smooth projector functions $\{\tilde{p}_\alpha^a\}$ is defined as

$$\langle \tilde{p}_\alpha^a| \equiv \sum_\beta (\langle p^a | \tilde{\phi}^a \rangle)_{\alpha\beta}^{-1} \langle p_\beta^\alpha| \tag{2.13}$$

It can be shown that similar to $\{p_\alpha^a\}$, the smooth projector functions $\{\tilde{p}_\alpha^a\}$ have the following properties

$$\langle \tilde{p}_\beta^a | \tilde{\phi}_\alpha^a \rangle = \delta_{\alpha\beta} \tag{2.14}$$

$$\tilde{p}_\alpha^a(\mathbf{r}) = 0, \quad \forall \mathbf{r} \subset \Omega_a \tag{2.15}$$

Furthermore, it is straightforward to prove that

$$\langle \tilde{p}_\alpha^a| = \langle p_\alpha^a | \mathrm{Y}^{-1}$$

and therefore the local basis expansion coefficients (2.7) and the remainder Δ_n^a (2.8) can be alternatively represented as

$$c_{n,\alpha}^a = \langle \tilde{p}_\alpha^a | \tilde{\Psi}_n \rangle \tag{2.16}$$

$$|\Delta_n^a\rangle = (1 - \sum_\alpha |\tilde{\phi}_\alpha^a\rangle\langle \tilde{p}_\alpha^a|)|\tilde{\Psi}_n\rangle \tag{2.17}$$

The above two expressions show that if the basis $\{\phi_\alpha^a\}$ provides an accurate local representation for $\Psi_n(\mathbf{r})$, then the smooth basis $\{\tilde{\phi}_\alpha^a\}$ provides an accurate local representation for $\tilde{\Psi}_n(\mathbf{r})$ and vice versa. This is an important observation, since it is our objective to completely eliminate $\Psi_n(\mathbf{r})$ and seek for $\tilde{\Psi}_n(\mathbf{r})$ directly (see section 2.3).

From a practical point of view, it is the inverse transformation Y^{-1} that plays a major role in all the applications. The expression for Y^{-1} (2.12) involves basis sets $\{\phi_\alpha^a\}$ and $\{\tilde{\phi}_\alpha^a\}$ and smooth projector functions $\{\tilde{p}_\alpha^a\}$. The prescription for their construction is described in detail in section 3. Since for a given $\{\phi_\alpha^a\}$ and $\{\tilde{\phi}_\alpha^a\}$, there is a unique correspondence between $\{p_\alpha^a\}$ and $\{\tilde{p}_\alpha^a\}$, the smooth projector functions $\{\tilde{p}_\alpha^a\}$ can be generated directly based on (2.14) and (2.15). If desired, the projector functions $\{p_\alpha^a\}$ can then be found from

$$\langle p_\alpha^a| = \sum_\beta (\langle \tilde{p}^a | \phi^a \rangle)_{\alpha\beta}^{-1} \langle \tilde{p}_\beta^a| \tag{2.18}$$

Finally, we note that smooth wave functions are only generated for the valence states of the system. Since core states do not participate in the bonding, they are initially imported from the atomic calculations and kept frozen for the duration of the calculation. Accordingly, the additional requirement is imposed on $\{\phi_\alpha^a\}$ to be orthogonal to all the core states.

2.2. Expectation Values. *2.2.1. General Expression.* Consider the expectation value of the general local (or quasilocal) operator A with respect to a valence wave function Ψ

$$\langle A \rangle = \langle \Psi | \hat{A} | \Psi \rangle \tag{2.19}$$

Since, as we mentioned before, the wave function Ψ is highly oscillating in the atomic sphere region, the accurate evaluation of the expectation value in plane wave basis is impractical. Let us rewrite (2.19) in terms of the smooth wave function $\tilde{\Psi}$. Using (2.2) and (2.12) we find

$$\langle A \rangle = \langle \tilde{\Psi} | A | \tilde{\Psi} \rangle + \tag{2.20}$$

$$\sum_a \sum_{\alpha\beta} (\langle \tilde{\Psi} | \tilde{p}_\alpha^a \rangle (\langle \phi_\alpha^a | A | \phi_\beta^a \rangle - \langle \tilde{\phi}_\alpha^a | A | \tilde{\phi}_\beta^a \rangle) \langle \tilde{p}_\beta^a | \tilde{\Psi} \rangle) \tag{2.21}$$

$$+ \Delta\langle A \rangle \tag{2.22}$$

where

$$\Delta\langle A \rangle = \sum_a [\sum_\alpha c_\alpha^a (\langle \phi_\alpha^a| - \langle \tilde{\phi}_\alpha^a|)] A | \Delta^a \rangle + \sum_a \langle \Delta^a | A [\sum_\alpha (|\phi_\alpha^a\rangle - |\tilde{\phi}_\alpha^a\rangle) c_\alpha^a] \tag{2.23}$$

and Δ^a is given by (2.8) or (2.17). The original expression for expectation value now splits into several parts. The first part is a simple expectation value over the smooth wave function $\tilde{\Psi}$ which can be accurately calculated using plane wave basis. The troublesome high frequency components are now hidden in the second term. *This term, however, is one-center and restricted*

to atomic spheres region; thus, it can be easily precomputed on the radial grids around the atoms. The last term $\Delta(A)$ appears as a result of incompleteness of the local basis representation and goes to zero as the size the local basis increases. Furthermore, since the local basis representation is more accurate near the origin of the atom, we expect $\Delta^a(\mathbf{r})$ become larger away from the atom center. However, (2.9) shows that $(\phi^a_\alpha(\mathbf{r}) - \tilde{\phi}^a_\alpha(\mathbf{r}))$ has quite the opposite behavior, and the overlap and therefore the correction $\Delta\langle A\rangle$ is expected to be small. In our calculations the effect of $\Delta\langle A\rangle$ is neglected and the expectation value is calculated according to

$$\langle A\rangle \approx \langle\tilde{\Psi}|A|\tilde{\Psi}\rangle + \sum_a\sum_{\alpha\beta}(\langle\tilde{\Psi}|\tilde{p}^a_\alpha\rangle(\langle\phi^a_\alpha|A|\phi^a_\beta\rangle - \langle\tilde{\phi}^a_\alpha|A|\tilde{\phi}^a_\beta\rangle)\langle\tilde{p}^a_\beta|\tilde{\Psi}\rangle) \quad (2.24)$$

2.2.2. Orthogonality. Setting the operator A to the identity,

$$\langle\mathbf{r}|\hat{A}|\mathbf{r}'\rangle = \delta(\mathbf{r}-\mathbf{r}')$$

reveals that the orthogonality properties of smooth wave functions $\{\tilde{\Psi}_n\}$ are different from those of $\{\Psi_n\}$. Namely, if

$$\langle\Psi_i|\Psi_j\rangle = \delta_{ij}$$

then

$$\langle\tilde{\Psi}_i|O|\tilde{\Psi}_j\rangle = \delta_{ij} \quad (2.25)$$

Here the overlap operator is given by

$$O = 1 + \sum_a\sum_{\alpha\beta}|\tilde{p}^a_\alpha\rangle(\langle\phi^a_\alpha|\phi^a_\beta\rangle - \langle\tilde{\phi}^a_\alpha|\tilde{\phi}^a_\beta\rangle)\langle\tilde{p}^a_\beta| \quad (2.26)$$

2.2.3. Electron Density. The relationship between the valence electron density

$$n(\mathbf{r}) = \sum_n f_n|\Psi_n(\mathbf{r})|^2$$

and its smooth image

$$\tilde{n}(\mathbf{r}) = \sum_n f_n|\tilde{\Psi}_n(\mathbf{r})|^2$$

can be obtained from (2.24) by setting

$$\hat{A} = |\mathbf{r}\rangle\langle\mathbf{r}|$$

We obtain

$$n(\mathbf{r}) = \tilde{n}(\mathbf{r}) + \sum_a[n^a(\mathbf{r}-\mathbf{R}_a) - \tilde{n}^a(\mathbf{r}-\mathbf{R}_a)] \quad (2.27)$$

where one-center atomic densities $n^a(\mathbf{r})$ and $\tilde{n}^a(\mathbf{r})$ are given by

$$n^a(\mathbf{r}) = \sum_n f_n|\sum_\alpha c^a_{n\alpha}\,\phi^a_\alpha(\mathbf{r})|^2$$

$$\tilde{n}^a(\mathbf{r}) = \sum_n f_n|\sum_\alpha c^a_{n\alpha}\,\tilde{\phi}^a_\alpha(\mathbf{r})|^2$$

From (2.6) and (2.10) it is straightforward to prove that as $\Delta^a_n \to 0$

$$n^a(\mathbf{r}) \to n(\mathbf{r}), \quad \forall\mathbf{r}\subset\Omega_a$$

$$\tilde{n}^a(\mathbf{r}) \to \tilde{n}(\mathbf{r}), \quad \forall\mathbf{r}\subset\Omega_a$$

The above approximate relationships will be used in the sections that follow.

The decomposition into smooth and atomic densities can also be enforced for the frozen total core density $n_c(\mathbf{r}) = \sum_a n^a_c(\mathbf{r}-\mathbf{R}^a)$

$$n_c(\mathbf{r}) = \tilde{n}_c(\mathbf{r}) + \sum_a[n^a_c(\mathbf{r}-\mathbf{R}_a) - \tilde{n}^a_c(\mathbf{r}-\mathbf{R}_a)] \quad (2.28)$$

where $\tilde{n}_c(\mathbf{r}) = \sum_a\tilde{n}^a_c(\mathbf{r}-\mathbf{R}^a)$. The atom core density $n^a_c(\mathbf{r})$ is determined from a separate isolated atom calculation. The choice of the smooth counterpart $\tilde{n}^a_c(\mathbf{r})$ is fairly arbitrary aside from the requirements that it has to match $n^a_c(\mathbf{r})$ outside the atomic sphere and be smooth inside the sphere. In our calculations we use a Gaussian form

$$\tilde{n}_c(\mathbf{r}) = \alpha e^{-\beta r^2}/(4\pi)$$

with constants α and β determined by matching $n^a_c(\mathbf{r})$ and $\tilde{n}_c(\mathbf{r})$ differentiably at the surface of the atomic sphere.

2.2.4. Kinetic Energy. Using (2.24) with $A = -1/2\nabla^2$ the expression for the kinetic energy (1.2) follows directly as

$$T = \tilde{T} + \sum_a(T^a - \tilde{T}^a) + T_c \quad (2.29)$$

where

$$\tilde{T} = \sum_n f_n\left\langle\tilde{\Psi}_n\right|-\frac{1}{2}\nabla^2\left|\tilde{\Psi}_n\right\rangle$$

and

$$T^a = \sum_n\sum_{\alpha\beta}f_n c^{a*}_{n\alpha}\left\langle\phi^a_\alpha\right|-\frac{1}{2}\nabla^2\left|\phi^a_\beta\right\rangle c^a_{n\beta}$$

$$\tilde{T}^a = \sum_n\sum_{\alpha\beta}f_n c^{a*}_{n\alpha}\left\langle\tilde{\phi}^a_\alpha\right|-\frac{1}{2}\nabla^2\left|\tilde{\phi}^a_\beta\right\rangle c^a_{n\beta}$$

Here f_n denotes the occupation of state n. The core kinetic energy is contained in T_c and is imported from an isolated atom calculation.

2.2.5. Hartree Energy. Using (2.27) and (2.28) the Hartree energy (1.3) can written as

$$W = \frac{1}{2}\int\int\frac{(\tilde{n}(\mathbf{r})+\tilde{n}_c(\mathbf{r}))(\tilde{n}(\mathbf{r}')+\tilde{n}_c(\mathbf{r}'))}{|\mathbf{r}-\mathbf{r}'|}d\mathbf{r}d\mathbf{r}' + \sum_a\int\int\frac{(\tilde{n}(\mathbf{r})+\tilde{n}_c(\mathbf{r}))n^a_{loc}(\mathbf{r}')}{|\mathbf{r}-\mathbf{r}'|}d\mathbf{r}d\mathbf{r}' + \frac{1}{2}\sum_a\sum_{a'}\int\int\frac{n^{a'}_{loc}(\mathbf{r})n^a_{loc}(\mathbf{r}')}{|\mathbf{r}-\mathbf{r}'|}d\mathbf{r}d\mathbf{r}' \quad (2.30)$$

where $n^a_{\rm loc}(\mathbf{r})$ is defined as

$$n^a_{\rm loc}(\mathbf{r}) = n^a(\mathbf{r}) - \tilde{n}^a(\mathbf{r}) + n^a_{\rm c}(\mathbf{r}) - \tilde{n}^a_{\rm c}(\mathbf{r}) - n^a_{\rm Z}(\mathbf{r}) \tag{2.31}$$

It is important to realize that since

$$n^a(\mathbf{r}) = \tilde{n}^a(\mathbf{r}), \quad \forall \mathbf{r} \subset \Omega_{\rm I}$$

$$n^a_{\rm c}(\mathbf{r}) = \tilde{n}^a_{\rm c}(\mathbf{r}), \quad \forall \mathbf{r} \subset \Omega_{\rm I}$$

the density $n^a_{\rm loc}(\mathbf{r})$ is localized within the atomic sphere Ω_a. The interaction of localized charge densities $\{n^a_{\rm loc}(\mathbf{r})\}$ on the *different* atoms depends only on the overall multipole moments of $\{n^a_{\rm loc}(\mathbf{r})\}$ and not on its actual functional form. Thus, it is helpful to introduce a localized compensation charge density $n^a_{\rm cmp}(\mathbf{r})$ that has the same multipole moments as $n^a_{\rm loc}(\mathbf{r})$,

$$\int_{\Omega_a} r^l n^a_{\rm cmp}(\mathbf{r})\, Y^*_{lm}(\hat{\mathbf{r}})\, d\mathbf{r} = \int_{\Omega_a} r^l n^a_{\rm loc}(\mathbf{r})\, Y^*_{lm}(\hat{\mathbf{r}})\, d\mathbf{r} \tag{2.32}$$

and a simple analytical form:

$$n^a_{\rm cmp}(\mathbf{r}) = \sum_{lm} g^a_{lm}(\mathbf{r})\, Q^a_{lm} \tag{2.33}$$

Here $g^a_{lm}(\mathbf{r})$ represents a Gaussian function centered on atom a

$$g^a_{lm}(\mathbf{r}) = g_l(r)\, Y_{lm}(\theta,\varphi) = C^a_l r^l e^{-(r/\sigma^a)^2} Y_{lm}(\theta,\varphi) \tag{2.34}$$

The width of the Gaussian σ^a is chosen such that the compensation charge density $n^a{}_{\rm cmp}(\mathbf{r})$ is completely localized within the atomic region. The normalization constant C^a_l is fixed by the requirement that

$$\int g^a_{lm}(\mathbf{r}) r^l Y^*_{lm}(\theta,\varphi)\, d\mathbf{r} = 1$$

which leads to

$$C^a_l = \frac{2^{l+2}}{\sqrt{\pi}(2l+1)!!(\sigma^a)^{2l+3}} \tag{2.35}$$

The coefficients Q^a_{lm} in (2.33) are determined from (2.32) as

$$Q^a_{lm} = \int_{\Omega_a} r^l n^a_{\rm loc}(\mathbf{r})\, Y^*_{lm}(\hat{\mathbf{r}})\, d\mathbf{r} \tag{2.36}$$

Since multipole moments of $n^a_{\rm loc}(\mathbf{r})$ and $n^a_{\rm cmp}(\mathbf{r})$ are the same, we find that

$$\int\int \frac{n^{a'}_{\rm loc}(\mathbf{r})\, n^a_{\rm loc}(\mathbf{r}')}{|\mathbf{r}-\mathbf{r}'|} d\mathbf{r}d\mathbf{r}' = \int\int \frac{n^{a'}_{\rm cmp}(\mathbf{r})\, n^a_{\rm cmp}(\mathbf{r}')}{|\mathbf{r}-\mathbf{r}'|} d\mathbf{r}d\mathbf{r}', \quad \forall a \neq a'$$

Therefore, the Hartree energy (2.30) can be written as

$$W = \frac{1}{2}\int\int \frac{(\tilde{n}(\mathbf{r}) + \tilde{n}_{\rm c}(\mathbf{r}))(\tilde{n}(\mathbf{r}') + \tilde{n}_{\rm c}(\mathbf{r}'))}{|\mathbf{r}-\mathbf{r}'|} d\mathbf{r}d\mathbf{r}' + \int\int \frac{(\tilde{n}(\mathbf{r}) + n_{\rm c}(\mathbf{r}))n_{\rm cmp}(\mathbf{r}')}{|\mathbf{r}-\mathbf{r}'|} d\mathbf{r}d\mathbf{r}' + \sum_a \int\int \frac{(\tilde{n}(\mathbf{r}) + \tilde{n}_{\rm c}(\mathbf{r}))(n^a_{\rm loc}(\mathbf{r}') - n^a_{\rm cmp}(\mathbf{r}'))}{|\mathbf{r}-\mathbf{r}'|} d\mathbf{r}d\mathbf{r}' +$$

$$\frac{1}{2}\int\int \frac{n_{\rm cmp}(\mathbf{r})\, n_{\rm cmp}(\mathbf{r}')}{|\mathbf{r}-\mathbf{r}'|} d\mathbf{r}d\mathbf{r}' - \tag{2.37}$$

$$\frac{1}{2}\sum_a \int\int \frac{n^a_{\rm loc}(\mathbf{r})\, n^a_{\rm loc}(\mathbf{r}')}{|\mathbf{r}-\mathbf{r}'|} d\mathbf{r}d\mathbf{r}' \tag{2.38}$$

where $n_{\rm cmp}(\mathbf{r})$ is given by

$$n_{\rm cmp}(\mathbf{r}) = \sum_a n^a_{\rm cmp}(\mathbf{r} - \mathbf{R}^a)$$

Substituting back the explicit expression for $n^a_{\rm loc}(\mathbf{r})$ (see (2.31)), we obtain

$$W = \tilde{W} + \sum_a (W_a - \tilde{W}_a) + \Delta W \tag{2.39}$$

where

$$\tilde{W} = \frac{1}{2}\int\int \times \frac{(\tilde{n}(\mathbf{r}) + \tilde{n}_{\rm c}(\mathbf{r}) + n_{\rm cmp}(\mathbf{r}))(\tilde{n}(\mathbf{r}') + \tilde{n}_{\rm c}(\mathbf{r}') + n_{\rm cmp}(\mathbf{r}'))}{|\mathbf{r}-\mathbf{r}'|} d\mathbf{r}d\mathbf{r}' \tag{2.40}$$

$$W^a = \frac{1}{2}\int_{\Omega_a}\int_{\Omega_a} \times \frac{(n^a(\mathbf{r}) + n^a_{\rm c}(\mathbf{r}) - n^a_{\rm Z}(\mathbf{r}))(n^a(\mathbf{r}') + n^a_{\rm c}(\mathbf{r}') - n^a_{\rm Z}(\mathbf{r}'))}{|\mathbf{r}-\mathbf{r}'|} d\mathbf{r}d\mathbf{r}'$$

$$\tilde{W}^a = \frac{1}{2}\int_{\Omega_a}\int_{\Omega_a} \times \frac{(\tilde{n}^a(\mathbf{r}) + \tilde{n}^a_{\rm c}(\mathbf{r}) + n^a_{\rm cmp}(\mathbf{r}))(\tilde{n}^a(\mathbf{r}') + \tilde{n}^a_{\rm c}(\mathbf{r}') + n^a_{\rm cmp}(\mathbf{r}'))}{|\mathbf{r}-\mathbf{r}'|} d\mathbf{r}d\mathbf{r}'$$

$$\Delta W = \sum_a \int_{\Omega_a}\int_{\Omega_a} \times \frac{(\tilde{n}(\mathbf{r}) - \tilde{n}^a(\mathbf{r}) + \tilde{n}_{\rm c}(\mathbf{r}) - \tilde{n}^a_{\rm c}(\mathbf{r}))(n^a_{\rm loc}(\mathbf{r}') - n^a_{\rm cmp}(\mathbf{r}'))}{|\mathbf{r}-\mathbf{r}'|} d\mathbf{r}d\mathbf{r}' \tag{2.41}$$

The smooth Hartree energy $\tilde{W}$ cannot be readily evaluated in plane wave basis set, since the accurate representation of compensation charge density $n_{\rm cmp}(\mathbf{r})$ would require a large number of plane waves. The solution to this problem is found by introducing a smooth compensation charge $\tilde{n}_{\rm cmp}(\mathbf{r})$. It has the same structure as $n_{\rm cmp}(\mathbf{r})$,

$$\tilde{n}_{\rm cmp}(\mathbf{r}) = \sum_a \sum_{lm} \tilde{g}^a_{lm}(\mathbf{r})\, Q^a_{lm}$$

but the width the Gaussian $\tilde{g}^a_{lm}$ is larger than that of g^a_{lm} which makes $\tilde{n}_{\rm cmp}(\mathbf{r})$ smoother. Rewriting (2.40) in terms of $\tilde{n}_{\rm cmp}(\mathbf{r})$

we obtain

$$\tilde{W} = \frac{1}{2}\int\int \times \frac{(\tilde{n}(\mathbf{r}) + \tilde{n}_c(\mathbf{r}) + \tilde{n}_{cmp}(\mathbf{r}))(\tilde{n}(\mathbf{r}') + \tilde{n}_c(\mathbf{r}') + \tilde{n}_{cmp}(\mathbf{r}'))}{|\mathbf{r} - \mathbf{r}'|}d\mathbf{r}d\mathbf{r}' + \int\int \frac{(\tilde{n}(\mathbf{r}) + \tilde{n}_c(\mathbf{r}) + \tilde{n}_{cmp}(\mathbf{r}))(n_{cmp}(\mathbf{r}') - \tilde{n}_{cmp}(\mathbf{r}'))}{|\mathbf{r} - \mathbf{r}'|}d\mathbf{r}d\mathbf{r}' + \frac{1}{2}\int \frac{(n_{cmp}(\mathbf{r}) - \tilde{n}_{cmp}(\mathbf{r}))(n_{cmp}(\mathbf{r}') - \tilde{n}_{cmp}(\mathbf{r}'))}{|\mathbf{r} - \mathbf{r}'|}d\mathbf{r}d\mathbf{r}' \quad (2.42)$$

The first and the second terms in (2.42) can now be accurately evaluated using plane wave basis set, whereas the last term is calculated analytically using

$$\int\int \frac{g^{a_1}_{l_1m_1}(\mathbf{r}_1 - \mathbf{R})g^{a_2}_{l_2m_2}(\mathbf{r}_2)}{|\mathbf{r}_1 - \mathbf{r}_2|}d\mathbf{r}_1 d\mathbf{r}_2 = (-1)^{l_2}\sum_{lm}\frac{R^l i^{l_1+l_2+l}}{\sigma^{l+l_1+l_2+1}}\frac{(2\pi)^{5/2}\,2^{-(l+l_1+l_2+2)/(2)}\Gamma\left(\frac{l+l_1+l_2}{2}+\frac{1}{2}\right)}{\Gamma\left(l_1+\frac{3}{2}\right)\Gamma\left(l_2+\frac{3}{2}\right)\Gamma\left(l+\frac{3}{2}\right)} [(-1)^{m_1}G^{lm}_{l_1-m_1,l_2m_2}]Y_{lm}(\hat{\mathbf{R}})M\left(\frac{l+l_1+l_2}{2}+\frac{1}{2}, l+\frac{3}{2}, -\frac{R^2}{2\sigma^2}\right) \quad (2.43)$$

where $\sigma^2 = [(\sigma^{a_1})^2 + (\sigma^{a_2})^2]/2$, $M(a,b,z)$ is a Kummer's function,[1] and $G^{l,m}_{l_i,m_i;l_j,m_j}$ is a Gaunt coefficient

$$G^{l,m}_{l_i,m_i;l_j,m_j} = \int Y^*_{lm}(\hat{\mathbf{r}})Y_{l_i,m_i}(\hat{\mathbf{r}})Y^*_{l_j,m_j}(\mathbf{r})d\hat{\mathbf{r}} \quad (2.44)$$

Note that decomposition (2.42) is slightly different from the one given by Blöchl.

Lastly we would like to discuss the correction ΔW (see (2.41)) which is neglected in our calculations. There are two effects that contribute to its appearance. First is the overlap of the smooth atomic core densities, i.e.,

$$\tilde{n}_c(\mathbf{r}) \neq \tilde{n}^a_c(\mathbf{r}), \quad \forall \mathbf{r} \in \Omega_a$$

In all our cases this overlap was negligible. Second effect is due to the incompleteness of the local basis set that results in the difference between the smooth density $\tilde{n}(\mathbf{r})$ and its one-center expansion $\tilde{n}^a(\mathbf{r})$:

$$\tilde{n}(\mathbf{r}) - \tilde{n}^a(\mathbf{r}) = 2Re[\sum_{\alpha} c^a_{n,\alpha}\langle\tilde{\phi}^a_\alpha|\Delta^a_n\rangle] + |\Delta^a_n(\mathbf{r})|^2 \quad (2.45)$$

Being proportional to $\Delta^a_n(\mathbf{r})$ this difference goes with to zero as the size of the basis increases. Furthermore, in the expression for ΔW the effect of (2.45) is suppressed by integration with potential

$$\int_{\Omega_a}\frac{n^a_{loc}(\mathbf{r}') - n^a_{cmp}(\mathbf{r}')}{|\mathbf{r} - \mathbf{r}'|}d\mathbf{r}'$$

which is zero near the surface of the sphere, the place where $\tilde{n}(\mathbf{r}) - \tilde{n}^a(\mathbf{r})$ is at maximum.

2.2.6. Exchange−Correlation Energy. In the region outside the atomic spheres the wave function $\tilde{\Psi}(\mathbf{r})$ coincides with $\Psi(\mathbf{r})$ and

$$n(\mathbf{r}) + n_c(\mathbf{r}) = \tilde{n}(\mathbf{r}) + \tilde{n}_c(\mathbf{r}), \quad \forall \mathbf{r} \in \Omega_I$$

Neglecting $\Delta^a_n(\mathbf{r})$ and the core overlap we can also establish that

$$n(\mathbf{r}) + n_c(\mathbf{r}) = n^a(\mathbf{r}) + n^a_c(\mathbf{r}), \quad \forall \mathbf{r} \in \Omega_a$$

Therefore the exchange−correlation energy (1.4) can written as

$$E_{xc} = \int_{\Omega_I}\epsilon_{xc}(\tilde{n} + \tilde{n}_c)(\tilde{n}(\mathbf{r}) + \tilde{n}_c(\mathbf{r}))\,d\mathbf{r} + \sum_a\int_{\Omega_a}\epsilon_{xc}(n^a(\mathbf{r}) + n^a_c(\mathbf{r}))(n^a(\mathbf{r}) + n^a_c(\mathbf{r}))\,d\mathbf{r}$$

Adding and subtracting

$$\sum_a\int_{\Omega_a}\epsilon_{xc}(\tilde{n} + \tilde{n}_c)(\tilde{n}(\mathbf{r}) + \tilde{n}_c(\mathbf{r}))\,d\mathbf{r} = \sum_a\int_{\Omega_a}\epsilon_{xc}(\tilde{n}^a + \tilde{n}^a_c)(\tilde{n}^a(\mathbf{r}) + \tilde{n}^a_c(\mathbf{r}))\,d\mathbf{r}$$

we obtain

$$E = \tilde{E}_{xc} + \sum_a(E^a_{xc} - \tilde{E}^a_{xc}) \quad (2.46)$$

where

$$\tilde{E}_{xc} = \int \epsilon_{xc}(\tilde{n} + \tilde{n}_c)(\tilde{n}(\mathbf{r}) + \tilde{n}_c(\mathbf{r}))\,d\mathbf{r}$$

$$E^a_{xc} = \int_{\Omega_a}\epsilon_{xc}(n^a + n^a_c)(n^a(\mathbf{r}) + n^a_c(\mathbf{r}))\,d\mathbf{r}$$

$$\tilde{E}^a_{xc} = \int_{\Omega_a}\epsilon_{xc}(\tilde{n} + \tilde{n}_c)(\tilde{n}(\mathbf{r}) + \tilde{n}_c(\mathbf{r}))\,d\mathbf{r}$$

2.3. Ground State Solution. Using (2.29), (2.39), and (2.46) the energy functional (1.1) can now be written in terms of $\{\tilde{\Psi}_n\}$ as

$$E[\{\tilde{\Psi}_n\}] = \tilde{T} + T_c + \tilde{W} + \tilde{E}_{xc} + \sum_a(T^a + W_a + E^a_{xc}) - \sum_a(\tilde{T}^a + \tilde{W}_a + \tilde{E}^a_{xc}) \quad (2.47)$$

To minimize the errors due to local basis incompleteness, it also suggested[7] to augment the energy functional (2.47) with the auxiliary pseudopotential energy term

$$V = \int(\sum_a \bar{v}^a(\mathbf{r}))(\tilde{n}(\mathbf{r}) + \tilde{n}_c(\mathbf{r})) - \sum_a\int \bar{v}^a(\mathbf{r})(\tilde{n}^a(\mathbf{r}) + \tilde{n}^a_c(\mathbf{r}))\,d\mathbf{r}$$

The potential $\bar{v}^a(\mathbf{r})$ is localized entirely within the atomic sphere, and the pseudopotential energy term V vanishes if the basis is complete and there is no core overlap.

Given the one-to-one correspondence between Ψ_n and $\tilde{\Psi}_n$, the ground state energy and density can now be found by minimizing the energy functional (2.47) with respect to $\tilde{\Psi}_n$

subject to the constraints (see (2.25))

$$\langle\tilde{\Psi}_i|O|\tilde{\Psi}_j\rangle = \delta_{ij} \tag{2.48}$$

Implementing the above constraints via Lagrange multipliers ϵ_{ij}, we obtain

$$\frac{\delta}{\delta\tilde{\Psi}_n}(E[\{\tilde{\Psi}_n\}] - \sum_{ij}\epsilon_{ij}\langle\tilde{\Psi}_i|O|\tilde{\Psi}_j\rangle) = 0 \tag{2.49}$$

Differentiation with respect to $\tilde{\Psi}_n$ yields the following Schrödinger-like equation

$$(\tilde{H} + \sum_a (H^a - \tilde{H}^a))|\tilde{\Psi}_i\rangle = \sum_j \epsilon_{ij} O|\tilde{\Psi}_j\rangle, \quad (i = 1, ..., N) \tag{2.50}$$

Via the unitary transformation among $\{\tilde{\Psi}_i\}$, the above equation can be cast into the form similar to (1.5) as

$$(\tilde{H} + \sum_a (H^a - \tilde{H}^a))|\tilde{\Psi}_i\rangle = \epsilon_i O|\tilde{\Psi}_i\rangle, \quad (i = 1, ..., N) \tag{2.51}$$

where $\{\epsilon_i\}$ are the eigenvalues of the Lagrange multiplier matrix ϵ_{ij}.

The smooth part of the Hamiltonian in (2.50) is given by

$$\tilde{H}(\mathbf{r}) = -\frac{1}{2}\nabla^2 + \tilde{v}(\mathbf{r})$$

where

$$\tilde{v}(\mathbf{r}) = \int \frac{\tilde{n}(\mathbf{r}') + \tilde{n}_c(\mathbf{r}') + n_{cmp}(\mathbf{r}')}{|\mathbf{r} - \mathbf{r}'|}d\mathbf{r}' + v_{xc}[\tilde{n} + \tilde{n}_c] + \sum_a \bar{v}^a(\mathbf{r})$$

The one-center atomic contributions are given by

$$H^a = \sum_a \sum_{\alpha\beta} |\tilde{p}^a_\alpha\rangle\langle\phi^a_\alpha|h_a + v^a_q|\phi^a_\beta\rangle\langle\tilde{p}^a_\beta| \tag{2.52}$$

$$\tilde{H}^a = \sum_a \sum_{\alpha\beta} |\tilde{p}^a_\alpha\rangle\langle\tilde{\phi}^a_\alpha|\tilde{h}_a + v^a_q + \bar{v}^a|\tilde{\phi}^a_\beta\rangle\langle\tilde{p}^a_\beta| \tag{2.53}$$

with

$$h_a(\mathbf{r}) = -\frac{1}{2}\nabla^2 + \int \frac{n^a - n^a_Z + n^a_c}{|\mathbf{r} - \mathbf{r}'|}d\mathbf{r}' + v_{xc}[n^a + n^a_c]$$

$$\tilde{h}^a(\mathbf{r}) = -\frac{1}{2}\nabla^2 + \int \frac{\tilde{n}^a + \tilde{n}^a_c + n^a_{cmp}}{|\mathbf{r} - \mathbf{r}'|}d\mathbf{r}' + v_{xc}[\tilde{n}^a + \tilde{n}^a_c]$$

The multipole potential

$$v^a_q(\mathbf{r}) = \sum_{lm} (v^a_q)^{lm} \mathbf{r}^l Y^*_{lm}(\hat{\mathbf{r}})$$

stems from the dependence of the total energy on the compensation charge density. The coefficients $(v^a_q)^{lm}$ are given by

$$(v^a_q)^{lm} = \int\int \frac{g^a_{lm}(\mathbf{r})(\tilde{n}(\mathbf{r}') + \tilde{n}_c(\mathbf{r}') + \tilde{n}_{cmp}(\mathbf{r}'))}{|\mathbf{r} - \mathbf{r}'|}d\mathbf{r}d\mathbf{r}' + \int\int \frac{\tilde{g}^a_{lm}(\mathbf{r})(n_{cmp}(\mathbf{r}') - \tilde{n}_{cmp}(\mathbf{r}'))}{|\mathbf{r} - \mathbf{r}'|}d\mathbf{r}d\mathbf{r}' + \int\int \frac{(g^a_{lm}(\mathbf{r}) - \tilde{g}^a_{lm}(\mathbf{r}))(n_{cmp}(\mathbf{r}') - \tilde{n}_{cmp}(\mathbf{r}'))}{|\mathbf{r} - \mathbf{r}'|}d\mathbf{r}d\mathbf{r}' - \int_{\Omega_a}\int_{\Omega_a} \frac{g^a_{lm}(\mathbf{r})(\tilde{n}^a(\mathbf{r}') + \tilde{n}^a_c(\mathbf{r}') + n^a_{cmp}(\mathbf{r}'))}{|\mathbf{r} - \mathbf{r}'|}d\mathbf{r}d\mathbf{r}'$$

The first two terms are evaluated using plane wave basis set; third term, analytically using (2.43); and the fourth term, on the radial grids around the atoms.

With the typical basis set size is of the order of tens of thousands plane waves a direct diagonalization of the equation (2.51) is impractical. The more sensible approach is to use one of the several iterative methods[19] to the minimization problem (2.50). A simple steepest descent method was used in this work. All of these methods require the calculation of the gradient

$$|G_n\rangle = \tilde{H}|\tilde{\Psi}_n\rangle + \sum_a (H^a - \tilde{H}^a)|\tilde{\Psi}_n\rangle$$

The smooth part of the gradient $\tilde{H}|\tilde{\Psi}_n\rangle$ can be found via standard technique found in pseudopotential methods.[20] Namely, given the wave function and the smooth potential $\tilde{v}(\mathbf{r})$, $G_n(\mathbf{k})$ can be evaluated as

$$G_n(\mathbf{k}) = -\frac{\mathbf{k}^2}{2}\tilde{\Psi}_n(\mathbf{k}) + \mathrm{FFT}[\tilde{v}(\mathbf{r})\tilde{\Psi}_n(\mathbf{r})]$$

where FFT[...] denotes fast Fourier transformation into **k** space. To calculate the local part of the gradient

$$|G^a_n\rangle \equiv (H^a - \tilde{H}^a)|\tilde{\Psi}_n\rangle \tag{2.54}$$

it is helpful to precompute the following matrix elements

$$(n^a)^{\ l}_{\alpha\beta} = \int_0^{r^a_c} \phi^a_{n_\alpha l_\alpha}(r)\phi^a_{n_\beta l_\beta}(r) r^l dr$$

$$(\tilde{n}^a)^{\ l}_{\alpha\beta} = \int_0^{r^a_c} \tilde{\phi}^a_{n_\alpha l_\alpha}(r)\tilde{\phi}^a_{n_\beta l_\beta}(r) r^l dr$$

$$(v^a_Z)_{\alpha\beta} = Z\delta_{m_\alpha m_\beta}\delta_{l_\alpha l_\beta}\int_0^{r^a_c} \frac{\phi^a_{n_\alpha l_\alpha}\phi^a_{n_\beta l_\beta}}{r}dr$$

$$(\tilde{v}^a)_{\alpha\beta} = \delta_{m_\alpha m_\beta}\delta_{l_\alpha l_\beta}\int_0^{r^a_c} \tilde{v}^a(r)\phi^a_{n_\alpha l_\alpha}\phi^a_{n_\beta l_\beta}dr$$

$$(v^a_{core})_{\alpha\beta} = \delta_{m_\alpha m_\beta}\delta_{l_\alpha l_\beta} 4\pi \int_0^{r^a_c}\int_0^{r^a_c} \frac{1}{r_>}\{\phi^a_{n_\alpha l_\alpha}(r)\phi^a_{n_\beta l_\beta}(r) n_c(r') - \tilde{\phi}^a_{n_\alpha l_\alpha}(r)\tilde{\phi}^a_{n_\beta l_\beta}(r)\tilde{n}_c(r')\}drdr'$$

$$(v^a_{comp})^{\ l}_{\alpha\beta} = \frac{4\pi}{2l+1}\int_0^{r^a_c}\int_0^{r^a_c} \tilde{\phi}^a_{n_\alpha l_\alpha}(r)\tilde{\phi}^a_{n_\beta l_\beta}(r)\frac{r^l_<}{r^{l+1}_>} g^a_l(r') r'^2 dr' dr$$

$$(t^a)_{\alpha\beta} = \frac{\delta_{m_\alpha m_\beta}\delta_{l_\alpha l_\beta}}{2}\int_0^{r^a_c}\left\{(\phi^a_{n_\alpha l_\alpha})'(\phi^a_{n_\beta l_\beta})' - (\tilde{\phi}^a_{n_\alpha l_\alpha})'(\tilde{\phi}^a_{n_\beta l_\beta})' + l_\alpha(l_\alpha+1)\frac{\phi^a_{n_\alpha l_\alpha}\phi^a_{n_\beta l_\beta} - \tilde{\phi}^a_{n_\alpha l_\alpha}\tilde{\phi}^a_{n_\beta l_\beta}}{r^2}\right\}dr$$

$$(\upsilon_H^a)^{\,l}_{\alpha\beta\mu\nu} = \frac{4\pi}{2l+1}\int_0^{r_c^a}\int_0^{r_c^a}\frac{r_<^l}{r_>^{l+1}}\{\phi^a_{n_\alpha l_\alpha}(r)\phi^a_{n_\beta l_\beta}(r)\phi^a_{n_\mu l_\mu}(r') \times \phi^a_{n_\nu l_\nu}(r') - \tilde{\phi}^a_{n_\alpha l_\alpha}(r)\tilde{\phi}^a_{n_\beta l_\beta}(r)\tilde{\phi}^a_{n_\mu l_\mu}(r')\tilde{\phi}^a_{n_\nu l_\nu}(r')\}\mathrm{d}r\mathrm{d}r'$$

where the following representation for PAW basis was assumed:

$$\phi^a_\alpha(\mathbf{r}) = \frac{\phi^a_{n_\alpha l_\alpha}(r)}{r}Y_{l_\alpha m_\alpha}(\theta,\varphi)$$

$$\tilde{\phi}^a_\alpha(\mathbf{r}) = \frac{\tilde{\phi}^a_{n_\alpha l_\alpha}(r)}{r}Y_{l_\alpha m_\alpha}(\theta,\varphi) \qquad (2.55)$$

$$\tilde{p}_\alpha(\mathbf{r}) = \frac{\tilde{p}^a_{n_\alpha l_\alpha}(r)}{r}Y_{l_\alpha m_\alpha}(\theta,\varphi)$$

with α as compound index ($n_\alpha l_\alpha m_\alpha$).

In this notation the local part of the gradient takes the form

$$G^a_n(\mathbf{r}) = \sum_{\alpha\beta}|\tilde{p}^a_\alpha\rangle(G^a_n)_{\alpha\beta}c^a_{n\beta}$$

where

$$(G^a_n)_{\alpha\beta} = (t^a)_{\alpha\beta} + (\upsilon^a_Z)_{\alpha\beta} + (\upsilon^a_{\mathrm{core}})_{\alpha\beta} + (\bar{v}^a)_{\alpha\beta} + \sum_{lm}G^{lm}_{l_\alpha m_\alpha, l_\beta m_\beta}Q^a_{lm}(\upsilon^a_{\mathrm{comp}})^{\,l}_{\alpha\beta} + \sum_{lm}G^{lm}_{l_\alpha m_\alpha, l_\beta m_\beta}(\upsilon^a_q)^{lm}((n^a)^{\,l}_{\alpha\beta} - (\tilde{n}^a)^{\,l}_{\alpha\beta}) + \sum_{lm}\sum_{l_\mu m_\mu l_\nu m_\nu}G^{lm}_{l_\alpha m_\alpha, l_\beta m_\beta}(\upsilon^a_H)^{\,l}_{\alpha\beta\mu\nu}\,G^{lm}_{l_\mu m_\mu, l_\nu m_\nu}\Big(\sum_{n'}f_{n'}c^{a*}_{n'\mu}\,c^a_{n'\nu}\Big) + \sum_{lm}G^{lm}_{l_\alpha m_\alpha, l_\beta m_\beta}(\upsilon^a_{\mathrm{xc}})^{\,lm}_{\alpha\beta}$$

Since Gaunt coefficient $G^{lm}_{l_\alpha m_\alpha, l_\beta m_\beta}$ (defined in (2.44)) is nonzero only if all the following conditions are satisfied:

$$m - m_\alpha + m_\beta = 0$$

$$|l_\alpha - l_\beta| \le l \le l_\alpha + l_\beta$$

$$\mathrm{mod}(l + l_\alpha + l_\beta, 2) = 0$$

the summation over orbital momenta can be greatly reduced. Currently the exchange−correlation matrix element $(\upsilon^a_{\mathrm{xc}})^{\,lm}_{\alpha\beta}$ is recalculated at each step in the self-consistent process as

$$(\upsilon^a_{\mathrm{xc}})^{\,lm}_{\alpha\beta} = \int_0^{r_c^a}[\phi^a_{n_\alpha l_\alpha}(r)\upsilon^{lm}_{\mathrm{xc}}(r)\phi^a_{n_\beta l_\beta}(r) - \tilde{\phi}^a_{n_\alpha l_\alpha}(r)\tilde{\upsilon}^{lm}_{\mathrm{xc}}(r)\tilde{\phi}^a_{n_\beta l_\beta}(r)]\,\mathrm{d}r$$

$$\upsilon^{lm}_{\mathrm{xc}}(r) = \int \upsilon_{\mathrm{xc}}[n^a + n^a_c]Y^*_{lm}(\hat{\mathbf{r}})\,\mathrm{d}\hat{\mathbf{r}}$$

$$\tilde{\upsilon}^{lm}_{\mathrm{xc}}(r) = \int \upsilon_{\mathrm{xc}}[\tilde{n}^a + \tilde{n}^a_c]Y^*_{lm}(\hat{\mathbf{r}})\,\mathrm{d}\hat{\mathbf{r}}$$

The calculation of $(\upsilon^a_{\mathrm{xc}})^{\,lm}_{\alpha\beta}$ can be simplified via Taylor expansion around the dominant $l = 0$ term.[7]

3. Generation of the Local Basis Set

Construction of the local basis set is an important step in the PAW method and determines the success of the subsequent calculations. In the present work we have closely followed the procedure suggested by Blöchl[7] (for other approaches see Holzwarth et al.[12,13]). To determine the local basis set $\{\phi^a_\alpha\}$, we performed a self-consistent spin-restricted spherically symmetric calculation for a given atom. This calculation provides the bound state valence orbitals that constitute the main part of the basis $\{\phi^a_\alpha\}$. The rest of the basis set $\{\phi^a_\alpha\}$ comes from scattering states at specific energies, which are obtained by the outward integration of the Schrödinger equation with the already determined Kohn−Sham potential. Once $\{\phi^a_\alpha\}$ is found, the smooth basis set $\{\tilde{\phi}^a_\alpha\}$ is constructed similar to the method that is used to obtain Hamman pseudopotential. Let $\upsilon^a(r)$ denote the Kohn−Sham potential obtained from the earlier calculation of $\{\phi^a_\alpha\}$:

$$\Big(-\frac{1}{2}\nabla^2 + \upsilon^a(r)\Big)\phi^a_\alpha(\mathbf{r}) = \epsilon^a_\alpha\,\phi^a_\alpha(\mathbf{r}) \qquad (3.1)$$

We now introduce a smooth potential $\tilde{\upsilon}^a(r)$ defined such that $\tilde{\upsilon}^a(r) \approx \upsilon^a(r)$ outside the atomic sphere radius R^a. The actual functional form of $\tilde{\upsilon}^a(r)$ inside the atomic sphere could be chosen in many different ways. In the present work for all the elements excluding transition elements we use

$$\tilde{\upsilon}^a(r) = (1 - \mathrm{e}^{-(r/r^a_k)^\lambda})\upsilon^a(r) + \tilde{\upsilon}_0\mathrm{e}^{-(r/r^a_k)^\lambda} \qquad (3.2)$$

where λ is usually set to 6 and the cutoff radius r^a_k is chosen such that $\mathrm{e}^{-(r/r_k)^\lambda} \approx 0$ for $r > R^a$. For transition metal elements we use

$$\upsilon^a(r) = \tilde{\upsilon}^a_0 + \tilde{\upsilon}^a_1 r^2 + \tilde{\upsilon}^a_2 r^4 \qquad (3.3)$$

where parameters $\tilde{\upsilon}_1$ and $\tilde{\upsilon}_2$ are adjusted such $\tilde{\upsilon}^a(r)$ merges smoothly into $\upsilon^a(r)$ on the surface of the sphere ($r = r^a_k$). In both cases the parameter $\tilde{\upsilon}^a_0$ varies for different elements and is used to improve the scattering properties. Once the smooth potential $\tilde{\upsilon}^a(r)$ is defined, the basis function, $\tilde{\phi}^a_\alpha(\mathbf{r})$, is found as solution of the differential equation

$$\Big(-\frac{1}{2}\nabla^2 + \tilde{\upsilon}^a(r) + c^a_i\mathrm{e}^{-(r/r^a_k)^\lambda} - \epsilon_i\Big)\tilde{\phi}^a_\alpha(\mathbf{r}) = 0 \qquad (3.4)$$

The parameter c^a_i is adjusted so that

$$\tilde{\phi}^a_\alpha(\mathbf{R}^a) = \phi^a_\alpha(\mathbf{R}^a)$$

$$\left.\frac{\mathrm{d}\tilde{\phi}^a_\alpha(\mathbf{r})}{\mathrm{d}\mathbf{r}}\right|_{r=R^a} = \left.\frac{\mathrm{d}\phi^a_\alpha(\mathbf{r})}{\mathrm{d}\mathbf{r}}\right|_{r=R^a}$$

Since potential $\upsilon^a(r)$ is spherically symmetric both $\tilde{\phi}^a_\alpha(\mathbf{r})$ and $\phi^a_\alpha(\mathbf{r})$ can be represented as

$$\tilde{\phi}^a_\alpha(\mathbf{r}) = \frac{\tilde{\phi}^a_{n_\alpha l_\alpha}(r)}{r}Y_{l_\alpha m_\alpha}(\hat{\mathbf{r}})$$

$$\phi^a_\alpha(\mathbf{r}) = \frac{\phi^a_{n_\alpha l_\alpha}(r)}{r}Y_{l_\alpha m_\alpha}(\hat{\mathbf{r}})$$

where nodal structure of $\tilde{\phi}^a_{n_\alpha l_\alpha}(r)$ is such that for given orbital momentum l_α the lowest energy orbital has zero nodes, the next lowest, one node, and so on.

The set of projector functions $\{\tilde{p}^a_\alpha\}$ is obtained from $\{\tilde{\phi}^a_\alpha\}$ as

$$\tilde{p}^a_\alpha(\mathbf{r}) = \Big(-\frac{1}{2}\nabla^2 + \tilde{\upsilon}^a(r) - \epsilon_i\Big)\tilde{\phi}^a_\alpha(\mathbf{r})$$

TABLE 1: Parameters Used in the Construction of Local Basis Set[a]

element	basis	R^a (au)	r_k^a (au)	σ^a (au)	$\tilde{v}0^a$ (au)
H[a]	1s	0.35	0.25	0.076	−3.43
H[b]	1s, 2p(0.0)	0.35	0.25	0.076	−3.43
Be	2s, 2p	2.28	1.62	0.544	0.64
C	2s, 2p	1.2	0.85	0.26	−2.80
O[a]	2s, 2p	1.09	0.89	0.24	−3.24
O[b]	2s ,2p, 3s(1.0), 3p(1.0)	1.09	0.89	0.24	−3.24
O[c]	2s, 2p, 3s(1.0), 3p(1.0), 3d(0.5)	1.09	0.89	0.24	−3.24
F[a]	2s, 2p	1.24	0.89	0.274	−1.93
F[b]	2s, 2p, 3s(0.0), 3p(1.0)	1.24	0.89	0.274	−1.81
F[c]	2s, 2p, 3s(0.0), 3p(1.0), 3d(0.0)	1.24	0.89	0.274	−1.81
Cr	3s, 3p, 3d, 4s, 4p, 4d(1.0)	1.49	1.10	0.326	−2.58
Fe	3s, 3p, 3d, 4s, 4p, 4d(1.0), 5s(1.0)	1.78	1.27	0.393	−2.99

[a] Numbers in round brackets in the second column denote the energy of the scattering states.

Since

$$\tilde{v}^a(r) = v^a(r), \quad \forall r > r_k^a$$

it follows from (3.4) that $\{\tilde{p}_\alpha^a\}$ are indeed localized within the atomic sphere region. Finally we used the Gram−Schmidt method[7] to transform all three sets $\{\phi_\alpha^a\}$, $\{\tilde{\phi}_\alpha^a\}$, and $\{\tilde{p}_\alpha^a\}$ such that

$$\int (\tilde{p}_\alpha^a(\mathbf{r}))^* \tilde{\phi}_\beta^a(\mathbf{r}) = \delta_{\alpha\beta}$$

Note that this last step scrambles basis sets $\{\phi_\alpha^a\}$ and $\{\tilde{\phi}_\alpha^a\}$ and that they no longer satisfy (3.1) and (3.4).

Additional quantities that are determined in this part of the calculations are the core densities $n_c^a(r)$, $\tilde{n}_c^a(r)$, the width of the compensation charge σ^a, and the local potential $\bar{v}^a(r)$. The smooth core density is chosen to be of the form

$$\tilde{n}_c(r) = \alpha e^{-\beta r^2}/(4\pi) \tag{3.5}$$

It is matched to true core density $n_c(r)$ at the radius R^a:

$$\tilde{n}_c(R^a) = n_c(R^a)$$

$$\left.\frac{d\tilde{n}_c(\mathbf{r})}{dr}\right|_{r=R^a} = \left.\frac{dn_c(r)}{dr}\right|_{r=R^a}$$

The compensation charge width σ^a is calculated such that the atom compensation charge density

$$n_{cmp}^a(\mathbf{r}) = g_{00}^a(\mathbf{r}) Q_{00}^a$$

is nearly zero at the surface of the atomic sphere. The multipole moment Q_{00}^a is determined as

$$Q_{00}^a = \frac{1}{\sqrt{4\pi}} \int_{\Omega_a} (n^a(r) - \tilde{n}^a(r) + n_c^a(r) - \tilde{n}_c^a(r))\, d\mathbf{r} - Z^a$$

where Z^a is the atomic charge and the densities $n^a(r)$ and $\tilde{n}^a(r)$ are obtained by summing over the *unscrambled* (before the Gram−Schmidt procedure above) valence orbitals and their smooth images

$$n^a(r) = \sum_\alpha f_\alpha |\phi_\alpha^a(r)|^2$$

$$\tilde{n}^a(r) = \sum_\alpha f_\alpha |\tilde{\phi}_\alpha^a(r)|^2$$

The local potential $\bar{v}(r)$ is obtained as

$$\bar{v}^a(r) = \tilde{v}^a(r) - \int \frac{\tilde{n}^a + \tilde{n}_c^a + n_{cmp}^a}{|\mathbf{r} - \mathbf{r}'|} d\mathbf{r}' - v_{xc}[\tilde{n}^a + \tilde{n}_c^a]$$

4. Results

In the following we assess the accuracy and efficiency of the PAW method by comparing the results with various other LSDA calculations such as norm-conserving pseudopotential, local basis, and finite grid calculations. The results we present here show that as far as numerical accuracy is concerned the method performs quite well. For a same number of plane waves our present PAW code is a factor of 1.5 slower than our most efficient pseudopotential code. The situation can certainly be improved since our pseudopotential code has been optimized by continuous use for the past several years, whereas the PAW code is still in the development stage. However, even at this level of performance, the PAW method has an advantage over norm-conserving pseudopotential methods for transition metal elements, since it requires a much smaller plane wave basis set.

Since our effort is to understand the convergence properties of the method rather than to predict properties, most of the molecules and atoms chosen for calculation have been selected because they have been extensively studied by other LSDA methods and because they present problem cases for the application of norm-conserving pseudopotentials. In all the calculations, the size of the cubic simulation cell was set at 20 au and the exchange−correlation functional was based on VWN parametrization.[24] It is well-known that the LSDA approximation significantly overestimates bond energies of diatomic molecules, especially in case of transition metal elements. As our objective was to observe the performance of PAW as a method for solving the LSDA equations, any discussions of improvements in LSDA, gradient corrections, etc., are left for future work.

4.1. Atoms. The accuracy of the PAW method depends on two factors: the completeness of the plane wave basis set with respect to the smooth wave functions $\{\tilde{\Psi}_n\}$ and the completeness of the local basis set $\{\phi_i^a\}$ in the atomic sphere region. The magnitude of these errors can be efficiently assessed by studying the results of PAW calculations for isolated atoms. (See Figure 1.)

The size of the plane wave basis is typically characterized by the energy cutoff, the kinetic energy of highest plane wave in the basis. As the energy cutoff increases, the errors due to incompleteness of the plane wave basis become smaller. However, a large energy cutoff can lead to unrealistically long execution times. In the PAW method the plane wave basis errors are determined the smoothness of basis set $\{\tilde{\phi}_\alpha^a\}$, since in order for various cancellations to occur the plane wave basis representation of $\{\tilde{\phi}_\alpha^a\}$ should be equivalent to that on the radial grid around the atom. The smoothness of the basis $\{\tilde{\phi}_\alpha^a\}$ depends on the size of the atomic sphere as well as the strength of the effective atomic potential. Our choice for the radius of the atomic sphere was around half the bond length of the corresponding homonuclear diatomic molecule. The convergence of total energy calculated with the PAW method as a function of the energy cutoff for various isolated atoms is shown in Figure 2.

As expected, the total energy errors correlate with the size of atomic spheres and the effective atomic charge. Owing to a large sphere size of 2.28 au and small effective charge, Be, which is easily handled by norm-conserving pseudopotential calculations,[25] achieves a 10^{-3} Ha (∼0.03 eV) error in total

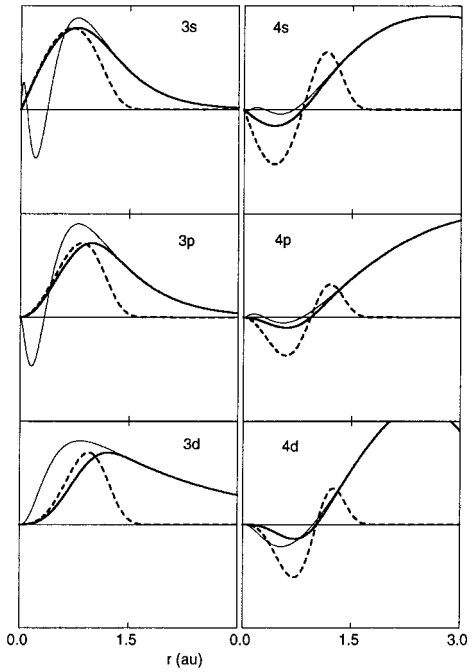

Figure 1. PAW basis for Cr: all-electron local basis functions, thin solid lines; smooth local basis, thick solid lines; projectors, dashed lines.

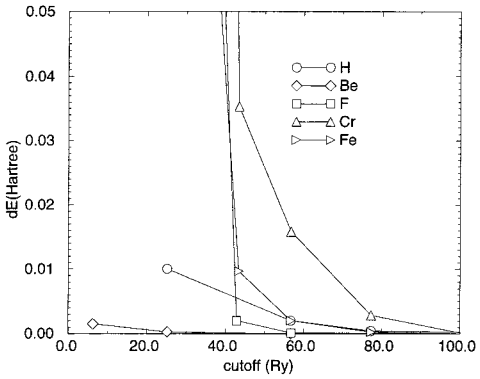

Figure 2. Plane wave convergence for the atomic total energies. d*E* defined as an absolute energy difference with the respect to the total energy at 100 Ry. Size of the simulation cell was set at 20 au.

energy with a cutoff of as little as 12 Ry. F represents an the extreme case of a system on the right-hand side of the periodic table, and in the first row, this element has a very high effective atom electron potential. Like other elements in the first row, the 2p orbital does not have to be orthogonal to an earlier p orbital and, therefore, effectively penetrates the core. Both these effects lead to the necessity of a strong norm-conserving pseudopotential for the p component of the wave function and resulting difficulties with plane wave convergence. In this case the PAW converges to a millihartree by 60 Ry. A similar convergence calculation[14] for the soft Troulier−Martins potential[22] (cutoff radius 1.2 au) requires 150 Ry, a cutoff which would lead to an very large plane wave basis. Transition metal element Cr, with the small sphere size of 1.49 au and a large effective charge, requires 80 Ry for an accuracy of two millihartree. This accuracy is beyond that of the LSDA approximation. Calculations including dynamics with 80 Ry cutoff are now appearing.[26,33] The above energy cutoffs can be reduced by increasing the size of the atomic sphere. However, large atomic sphere size can lead to overlap errors in dimers and cluster systems. It may also increase errors due to local basis incompleteness, since the local basis representation of the wave function will be required to cover a larger region of space.

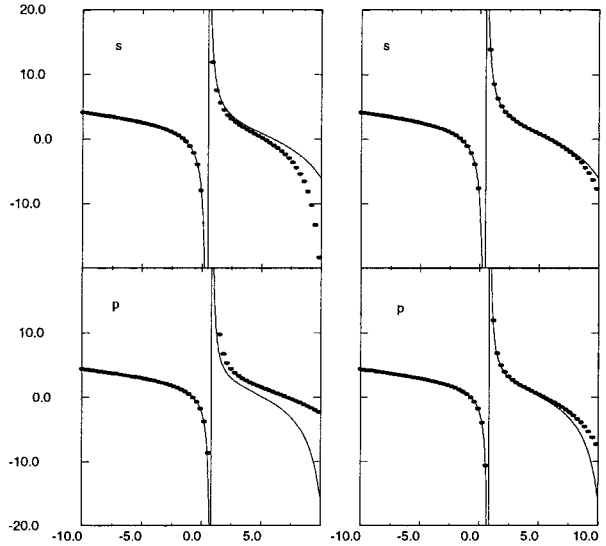

Figure 3. Comparison of the logarithmic derivatives of PAW and all-electron methods evaluated at the distance of 1.24 au. Left part refers to the setup F^a in Table 1; right part refers to the setup F^b in Table 1.

Similar to pseudopotentials, the PAW method will reproduce the isolated atom energies by construction. However, when the atom is inserted into the solid or molecule plane, the wave function will mix in a way different from that in the isolated atom. How well the correct (all-electron) mixing is reproduced in the new environment depends on the transferability of pseudopotential or the completeness of the local basis set in the PAW method. A common measure of the pseudopotential transferability is the comparison of the scattering properties of the pseudopotential and all-electron calculations. The same comparison in the PAW method serves a measure of the quality of the local basis representation of the PAW Hamiltonian. To perform this test, a scattered state problem for the PAW Hamiltonian is solved on a radial grid around the atom. The logarithmic derivative of the PAW scattering state is then compared to that of all-electron scattering state. Results of such calculations for the fluorine atom are shown in Figure 3. A minimal basis set (F^a set in Table 1), containing one function per angular momentum channel, provides a satisfactory description of the scattering properties (see left part in Figure 3). The scattering properties using an expanded basis set (F^b set in Table 1), containing two functions per angular momentum, are given in the right panel in Figure 3 and show convergence toward the all-electron result. The same trends have been observed for other elements, illustrating that the local basis description in the PAW method improves as the size of the basis set grows.

4.2. Homonuclear and Heteronuclear Diatomic Molecules. *4.2.1. Second-Row Dimers*. The second row diatomic molecules provide a good test for the PAW method, since these systems have been thoroughly investigated by a variety of LSDA methods.[4,16,21] Our main objectives were to assess the accuracy of the PAW method, the robustness with respect to different local basis sets, and the convergence with respect to the plane wave basis set. Since LSDA is used without gradient corrections in these calculations, the calculated bond energies reported are expected to be considerably larger than the experimental energy. Therefore, comparisons are made with the other LSDA calculations. Unless noted otherwise, all the LSDA calculations were based on VWN[24] parametrization of the exchange−correlation functional.

We start with an H_2 dimer. The highly localized nature of 1s orbital and small atomic radius requires a relatively large plane

TABLE 2: Spectroscopic Properties of H_2 Molecule ($^1\Sigma$) Calculated with Different LSDA Methods[a]

method	R (au)	D_e (eV)	w (cm^{-1})
this PAW (H[a])	1.46	4.86	4172
Gaussian[16]	1.45	4.91	4277
PAW (Blöchl)[7]	1.46	4.62	4040
finite grid[4]	1.45	4.9	4190

[a] PAW local basis set consisted of single 1s orbital, see Table 1. Blöchl's calculation uses Perdew−Zunger parametrization of the exchange−correlation functional.

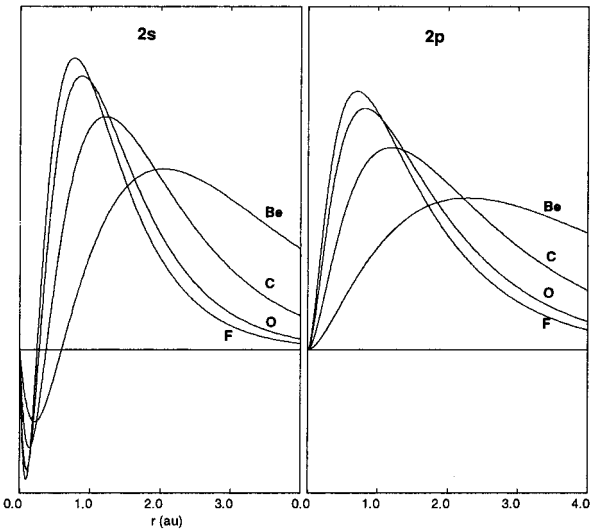

Figure 4. Localization of s and p orbitals for the second-row elements.

TABLE 3: Spectroscopic Properties of Be_2 Molecule ($^1\Sigma$) Calculated with Different LSDA Methods[a]

method	R (au)	D_e (eV)	w(cm^{-1})
this PAW	4.62	0.49	350
Gaussian[16]	4.63	0.5	362
PAW (Blöchl)[7]	4.51	0.53	367
finite grid[4]		0.56	

[a] PAW local basis set consisted of 2s, 2p orbitals, see Table 1. Blöchl's calculation uses Perdew−Zunger parametrization of the exchange−correlation functional.

wave basis set. In our calculation we used an energy cutoff of 60 Ry. The local basis consisted of single 1s orbital. As reported in Table 2, the PAW results agree very well with the other LSDA calculations.

Next we have calculated second-row homonuclear molecules, Be_2, C_2, O_2, and F_2, using 2s, 2p local basis set. The distinguishing feature of second-row elements is a gradual localization of 2s, 2p valence orbitals (see Figure 4) across the periodic table.

Located on the left-hand side of the periodic table, Be has fairly diffuse electronic states and can be easily treated via plane wave pseudopotential methods.[25] In our calculation of Be_2 (see Table 3) we have used a cutoff of 25 Ry. As one moves to the right the electronic states become more and more localized (see Figure 4), and by F the problem becomes quite difficult for norm-conserving pseudopotential methods. Such behavior can be accommodated by the PAW method since the rapidly varying localized components of the orbitals are projected out using the local basis set. In our calculations of C_2, O_2, and F_2 molecules (see Tables 4−6) we have used a cutoff of 60 Ry.

Overall, as the results in Tables 3−6 indicate, even with the small (2s, 2p) local basis set the PAW method can provide accurate LSDA results across the second row of the periodic table. The errors due to local basis set incompleteness (see (2.23)) in PAW method should become more accurate as the size of the basis increases. We have demonstrated before that the scattering properties of the fluorine atom improve as the local basis set grows. Here, we studied the change in the ground state properties of O_2, F_2 as the basis size increased. The results in Tables 7 and 8 indicate the addition of the 3s and 3p functions results in better agreement with the results by Painter and Averill[16] and Becke.[4] Further addition of 3d basis function has little effect. The improvement of the binding energy for a bigger basis set is only of the order of 0.1 eV. This means that the minimal 2s, 2p basis set already offers a good description of the atomic sphere region in the second-row elements.

We have also performed a PAW calculation of HF molecule. The energy cutoff was set at 60 Ry. Strong ionic character of this molecule serves as a good test of the accuracy and robustness of PAW local basis set. The local basis set for F consisted of 2s and 2p orbitals; the basis set for H was varied from single 1s orbital to 1s, 2p orbitals. In both cases, the PAW

TABLE 4: Spectroscopic Properties of C_2 Molecule ($^1\Sigma$) Calculated with Different LSDA Methods[a]

method	R (au)	D_e (eV)	w (cm^{-1})
this PAW	2.37	7.27	1736
finite grid[4]	2.35	7.3	1880
Gaussian[16]	2.36	7.19	1869
pseudopotential[26]	2.34	7.17	1849

[a] PAW local basis set consisted of 2s, 2p orbitals, see Table 1. Pseudopotential numbers correspond to psp 1 potential at 67 Ry.

TABLE 5: Spectroscopic Properties of O_2 Molecule ($^3\Sigma$) Calculated with Different LSDA Methods[a]

method	R (au)	D_e (eV)	w(cm^{-1})
this PAW	2.31	7.32	1571
PAW (Blöchl)[7]	2.32	7.33	1660
Gaussian[16]	2.30	7.54	1563
finite grid[4]	2.27	7.6	1620

[a] PAW local basis set consisted of 2s, 2p orbitals, see Table 1. Blöchl's calculation uses Perdew−Zunger parametrization of the exchange−correlation functional.

TABLE 6: Spectroscopic Properties of F_2 Molecule ($^1\Sigma$) Calculated with Different LSDA Methods[a]

method	R (au)	D_e (eV)	w (cm^{-1})
this PAW (F[a])	2.66	3.23	1106
PAW (Blöchl)[7]	2.67	3.11	1148
pseudopotential (118 Ry)[14]	2.58	3.30	
Gaussian[16]	2.62	3.32	1069
finite grid[4]	2.61	3.4	1060

[a] PAW local basis set consisted of 2s, 2p orbitals, see Table 1. Blöchl's calculation uses Perdew−Zunger parametrization of the exchange−correlation functional.

TABLE 7: Spectroscopic Properties of O_2 Molecule ($^3\Sigma$) for Different PAW Local Basis Sets

basis set	R (au)	D_e (eV)	w (cm^{-1})
2s, 2p	2.31	7.32	1571
2s, 2p, 3s(1.0), 3p(1.0)	2.30	7.42	1583
2s, 2p, 3s(0.0), 3p(1.0), 3d(0.5)	2.29	7.44	1582

TABLE 8: Spectroscopic Properties of F_2 Molecule ($^1\Sigma$) for Different PAW Local Basis Sets

basis set	R (au)	D_e (eV)	w (cm^{-1})
2s, 2p	2.66	3.23	1106
2s, 2p, 3s(0.0), 3p(1.0)	2.64	3.32	1108
2s, 2p, 3s(0.0), 3p(1.0), 3d(0.0)	2.64	3.33	1109

TABLE 9: Spectroscopic Properties of HF Molecule Calculated with Different LSDA Methods[a]

method	R (au)	D_e (eV)	w (cm^{-1})
PAW (H^a, F^a)	1.77	7.02	4192
PAW (H^b, F^a)	1.77	7.02	4182
finite grid[5]	1.77	7.0	4143
APW[21]	1.76	6.23	3990
pseudopotential (118 Ry)[14]	1.75	7.03	

[a] The APW calculation by Serena and Baratoff was based on Hedin and Lundqvist parametrization, and the rest of the calculations were based on VWN[24] parametrization of the exchange−correlation functional.

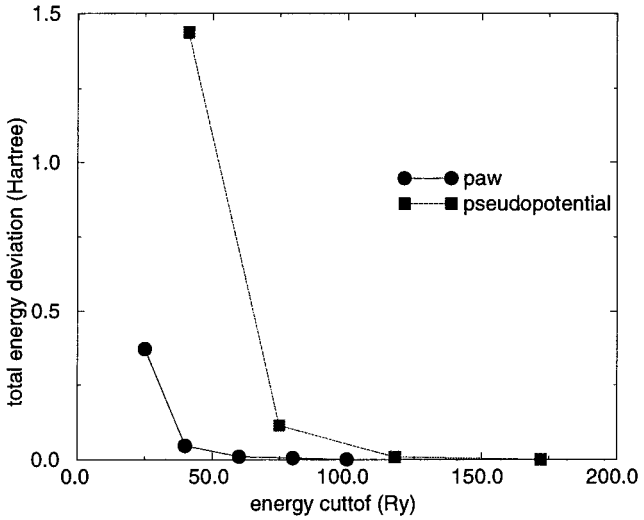

Figure 5. Comparision of the total energy convergence for F dimer using PAW method (setup F^a) and Troullier−Martin pseudopotential calculation.[17]

results agree very well with finite grid calculations by Becke[5] (see Table 4).

Since the norm conservation step is omitted while generating smooth local basis set $\{\tilde{\phi}_\alpha^a\}$, the PAW method is expected to yield a better convergence with respect to the size of the plane wave basis set than norm-conserving pseudopotential methods.[19] Using a minimal basis set consisting of 2s, 2p orbitals (setup F^a in Table 1), we have performed PAW calculation of the binding energy of F_2 for the plane wave basis sets with the different energy cutoffs. The comparison of these results with the similar plane wave pseudopotential calculations[14] is shown in Figure 5. The pseudopotential calculations were based on Troullier−Martin pseudopotential[22] with the cutoff radius of 1.2 au, which is close to PAW cutoff radius of 1.24 au. As shown on Figure 5, the PAW results were well converged within a millihartree by 60 Ry, whereas a cutoff of 140 Ry was necessary to get the same accuracy with the norm-conserving pseudopotential approach. This represents a substantial improvement in efficiency, since doubling the plane wave basis cutoff increases the number of plane waves in the basis by approximately a factor of three. Similar convergence has been observed when the local basis set was increased to include 3s, 3p orbitals. This is not surprising since the plane wave convergence depends on the smoothness of the auxiliary basis set $\{\tilde{\phi}_\alpha^a\}$ which is controlled by the size of the atomic sphere. Increase in the local basis set improves the approximation used to obtain (2.24).

It should be noted that the convergence of the pseudopotential methods can be greatly improved be removing the norm conservation condition via Vanderbilt's ultrasoft pseudopotentials.[23] As discussed by Blöchl[7] and later by Kresse and Joubert,[15] there are certain similarities between PAW method and ultrasoft pseudopotentials. From a numerical point of view both methods should have roughly the same efficiency. However, there are several advantages associated with all-electron nature of PAW approach. First, the issue of parameterizing the pseudopotential is avoided in PAW. This can be quite difficult in Vanderbilt's method.[15] Second, the accuracy of the PAW method (within the LSDA approximation) can by systematically improved by increasing the size of the local basis set. Third, the PAW method provides all-electron Kohn−Sham wave functions that are necessary in certain applications.[18]

TABLE 10: Equilibrium Properties of Cr_2 Molecule Calculated with Different LSDA Methods

	R (au)	D_e (eV)
PAW	3.05	3.1
finite grid[4]		3.0
DMOL[27a]	3.21	1.8
Gaussian (all-electron)[17]	3.27	2.4
Gaussian (with pseudopotential)[6]	3.21	2.8
Gaussian (all-electron)[3]	3.17	2.6
exptl	3.17	1.56

[a] DMOL calculation was based on von Barth−Hedin functional.

4.2.2. Transition Metal Dimers. The third-row transition metals are among the most difficult elements to describe with plane wave pseudopotential methods. These atoms contain $l = 0$ components with several nodes that extend to large distances as well as tightly bound (nodeless) $l = 2$ states that are well localized close to the core. For example, (see Figure 1), for Cr the 3d atomic functions has an outer maximum at about 1.3 au (see Figure 1) and the loosely bound 4s function has an outer maximum at 3 au. Simultaneous description of these two different length scales is difficult with norm-conserving pseudopotentials. The proper treatment of both 3d and 4s states is important in transition metal dimers. In addition there is a substantial overlap of localized 3d orbitals with the core states which makes separation of the core and valence density in pseudopotential calculations problematic.[2] As a result, the majority of ab initio calculations for these systems are performed using the local basis set methods.

In this work we have investigated two transition metal dimer systems, Cr_2 and Fe_2. In both calculations the energy cutoff was set at 60 Ry.

The chromium dimer Cr_2 has a short bond length of about 3.2 au, accordingly the atomic sphere radius for the generation of the PAW set was set to 1.5 au. At such small bond distance there is a significant overlap between 3s and 3p semicore states on the neighboring atoms, which prompted their inclusion in local basis set (see Table 1) along with 3d and 4s states. In agreement with the other LSDA calculations,[3] our PAW calculation reveals that for Cr_2, the ground state configuration,

$$\pi_u(d)^4\sigma_g(d)^2\delta_g(d)^4\sigma_g(s)^2$$

exhibits a spin symmetry breaking, i.e., in a given molecular orbital spin-up and spin-down electrons are concentrated on the opposite atoms in a dimer. The calculated equilibrium bond distance was 3.04 au with the binding energy of 3.24 eV. The comparison of these results with other calculations is given in Table 10. In all the calculations the LSDA approximation significantly overestimates the binding energy of Cr_2 as compared to the experimental value. Considering the rather large discrepancies in energy between the various local basis calculations the PAW calculation is within the accuracy of present LSDA calculations.

TABLE 11: Structural Properties of Fe_2 ($^7\Delta_u$) Molecule: Experimental Values as Cited in Reference 3

	R (au)	w (cm^{-1})
this PAW	3.70	464
Gaussian[9]	3.69	497
Blöchl PAW[7]	3.69	441
pseudopotential[2]	3.84	
exptl	3.53, 3.81	299.6

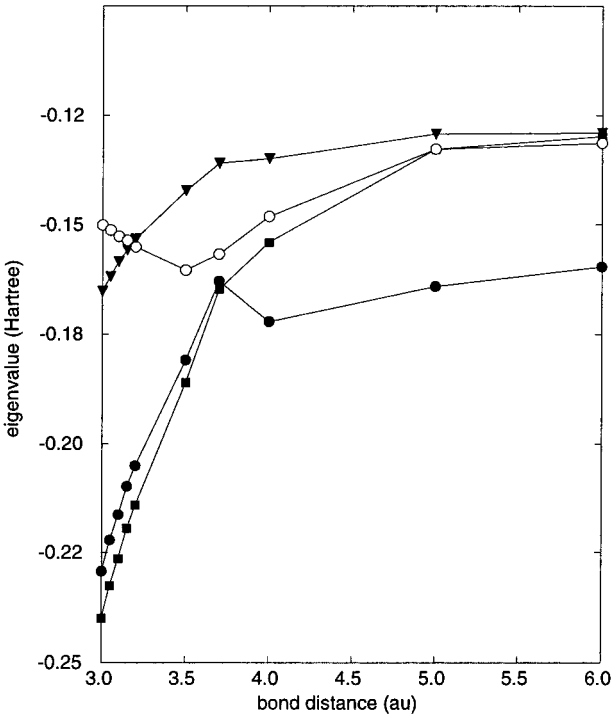

Figure 6. Molecular orbitals ordering for Cr dimer: squares correspond to π state, filled and opaque circles to σ states, triangles to δ state.

The different length scales of the 4s and 3d functions lead to an interesting variation in the molecular orbital ordering as a function of bond length. For small bond lengths, the 3d orbitals overlap strongly and the lowest molecular orbital has a large 3d component. On the other hand, for longer bond lengths the 4s interaction are strongest and the lowest molecular orbital has a large 4s component. To describe chemical processes with various bond lengths, it is important to get the right balance between 3d and 4s bonding. The orbital ordering for Cr_2 as a function of bond distance is given in Figure 6. The ordering predicted by PAW method agrees well with all-electron Gaussian calculation by Baykara, McMaster, and Salahub.[3] The crossover between lowest π and σ occurs around 3.6 au compared to 3.7 au as obtained by Baykara, McMaster, and Salahub.[3]

The Fe_2 dimer has a slightly larger bond length than Cr_2 which allows for a smoother basis. Consistent with local basis calculations PAW predicts that the lowest energy configuration in Fe_2 is ferromagnetic with the total spin 3 and the valence configuration given by

$$[1\sigma_g\pi_u^2\,\delta_g^2 2\sigma_g\delta_u^2\,\pi_g^2 1\sigma_u]^{\uparrow}[1\sigma_g\pi_u^2 2\sigma_g\delta_g]^{\downarrow}$$

The calculated bond distance of 3.70 au and frequency 464 cm^{-1}, which is in good agreement with other LSDA calculations.

There is less agreement regarding the LSDA values for the binding energy. The situation is complicated by the choice of the reference configuration of the isolated atom Fe($3d^64s^2$). As reported in Table 12, if no spherical symmetry is imposed on the reference atoms, we obtain the binding energy of 2.74 eV, which is close to the 2.89 eV result of Dhar and Kestner[29] who, as we understand, also did not impose any symmetry on the reference atom. Our binding energy with regard to spherically symmetric Fe atom is 4.49 eV, which is close to the 4.38 eV result of the Gaussian calculation of Castro, Jamorski, and Salahub[9] who also use spherically symmetric atom and the same VWN[24] parametrization of the exchange−correlation functional. This answer for the binding energy differs by 0.5 eV from the PAW result of Blöchl who has used a different local basis set (see Table 1 in ref 7) and a different (Perdew−Zunger) parametrization of the exchange−correlation functional. Similar to the case of Cr_2 LSDA value for binding energy again results in a severe overestimation of the experimental results (1.14 eV,[30] 1.30 eV[31]).

TABLE 12: Binding Energy of Fe_2 ($^7\Delta_u$) Molecule Calculated Using Different LSDA Methods

reference atoms	PAW	Gaussian[29]	Gaussian[9]	Blöchl[7]
spherical	4.49		4.38	3.99
nonspherical	2.74	2.89		

5. Conclusion

The accurate description of the potential surface between reacting species continues to be a central problem in the simulation of systems in which chemical change is important. Recent advances in electronic structure calculation using plane-wave methods has allowed the simulation of the dynamic behavior of complex systems directly on the ground state electronic surface.[32] These methods, while providing much new information on complex systems, are limited in their application. Essentially all the first principles methods for ab initio dynamics are based on plane wave solutions to the LSDA equations. For these solutions to be practical the plane wave expansions must be limited to the order of 500000 functions. For this to be case the wave function must be sufficiently smooth. For many elements this can be achieved by replacing the potential terms leading to the fast variation in the wave functions by smooth norm-conserving pseudopotentials. Pseudopotential methods are widely used and for some systems have been shown to have accuracies similar to all-electron LSDA methods.[26] Unfortunately, for some systems the atom electron interactions are so strong that it is difficult to find a pseudopotential that will allow a manageable plane wave solution. Important examples of such systems are the atoms first row atoms on the right side of the periodic table (O and F) and the transition metal elements. The transition metal elements are particularly difficult because they contain several length scales associated with the s, p, and d solutions to the LSDA equations. A number of articles have been published which address these problems.[34,35]

In this work we have studied the projected augmented wave method, an approach which is related to pseudopotential methods but takes a different path. In PAW method the rapidly varying portion of the wave function is projected out using local atomic basis set. The method, therefore, has some relation to the local basis methods that are widely used in quantum chemistry. The smooth remainder of the wave function is treated with plane waves essentially in the same way as in pseudopotential calculations. Since the local basis matrix elements can be precomputed, the efficiency of the PAW method should be similar to that of plane wave pseudopotential method. For large plane wave basis sets the most time-consuming parts in PAW method are the calculation of the local gradient (see (2.54)) and wave function orthogonalization. The calculation of the local

gradient scales as $N_a N_b N_g N_e$, where N_a number of atoms, N_b number of basis function per atom, N_g number of plane waves, and N_e number of electrons. This is similar in scaling to of nonlocal pseudopotential calculation in plane wave pseudopotential methods. The orthogonalization part scales as $N_e^2 N_g$. Since $N_g \sim N_a$ and $N_e \sim N_a$ both, local gradient part and orthogonalization will scale as third power of the number of atoms. At this stage of the development our PAW code is approximately 1.5 times slower than the highly optimized norm-conserving pseudopotential code.

The main difference between pseudopotential and PAW methods is that the latter is an all-electron method. No part of the valence orbitals is ever discarded but rather treated in different spaces. The local part of the Hamiltonian (see (2.52) and (2.53)) through the dependence on the orbitals can dynamically respond to the changes in environment. This should be contrasted with the pseudopotential methods where the pseudopotential is a static frozen quantity, imported from the isolated atom environment. The all-electron nature of the PAW method is also invaluable in other than ground state applications such excited state energies, polarizabilities, etc., which require the knowledge of all-electron orbitals. The core orbitals in PAW method are frozen but not ignored completely as typically done in pseudopotential methods. Considering the nonlinear nature of the exchange−correlation functional carrying the total density (valence plus frozen core) can be important factor for some systems.

Various approximations must be made to implement the PAW method, e.g., (33), but according to the results that we have presented in section 4 this does not impair the accuracy of PAW calculations and the numbers produced are of the same qualify as methods based on local expansions. For all the elements that we have studied the size of the plane wave basis can be kept at the practical level allowing efficient implementation in ab initio dynamics. We believe that with improvements in efficiency the PAW method should provide a very general and accurate approach to the simulation of the complex materials.

6. Acknowledgment

We thank the Office of Naval Research for providing us with support and computer time at Naval Research Center through ONR Grant N00014-97-1-0751. Additional support was received from LLNL Grant ICSR 98-11 and IUT B338397. We also thank E. Bylaska and R. Kawai for helpful discussions during the course of this work.

References and Notes

(1) Abramovitz, M.; Stegun, I. A. *Handbook of Mathematical Functions*; Dover Publications: New York, 1970.
(2) Ballone, P.; Jones, R. O. *Chem. Phys. Lett.* **1995**, *233*, 632.
(3) Baykara, N. A.; McMaster, B. N.; Salahub, D. R. *Mol. Phys.* **1984**, *52*, 891.
(4) Becke, A. D. *Phys. Rev.* **1986**, *A33*, 2786.
(5) Becke, A. D. *J. Chem. Phys.* **1992**, *97*, 9173.
(6) Bernholc, J.; Holzwarth, N. A. W. *Phys. Rev. Lett.* **1983**, *50*, 1451.
(7) Blöchl, P. E. *Phys. Rev.* **1994**, *B50*, 17953.
(8) Car, R.; Parrinello, M. *Phys. Rev. Lett* **1985**, *55*, 2471.
(9) Castro, M.; Jamorski, C.; Salahub, D. R. *Chem. Phys. Lett.* **1997**, *271*, 133.
(10) Delley, B. *J. Chem. Phys.* **1990**, *92*, 508.
(11) Dreizler, R. M.; Gross, E. K. U. *Density Functional Theory*; Springer-Verlag: New York, 1990.
(12) Holzwarth, N. A. W.; Matthews, G. E.; Dunning, R. B.; Tackett, A. R.; Zeng, Y. *Phys. Rev.* **1997**, *B55*, 2005.
(13) Holzwarth, N. A. W.; Matthews, G. E.; Tackett, A. R.; Dunning, R. B. *Phys. Rev.* **1998**, *B57*, 11827.
(14) Kawai, R. Private communication.
(15) Kresse, G.; Joubert, D. *Phys. Rev.* **1999**, *B59*, 1758.
(16) Painter, G. S.; Averill, F. W. *Phys. Rev.* **1982**, *B26*, 1781.
(17) Painter, G. S. *J. Phys. Chem.* **1986**, *90*, 5530.
(18) Petrilli, H. M.; Blöchl, P. E.; Blaha, P.; Schwartz, K. *Phys. Rev.* **1998**, *B57*, 14960.
(19) Pickett, W. E. *Comput. Phys. Rep.* **1989**, *9*, 115.
(20) Remler, D. K.; Madden, P. A. *Mol. Phys.* **1990**, *70*, 921.
(21) Serena, P. A.; Baratoff, A.; Soler, J. M. *Phys. Rev.* **1993**, *B48*, 2046.
(22) Troullier, N.; Martins, J. L. *Phys. Rev.* **1991**, *B43*, 1993.
(23) Vanderbilt, D. *Phys. Rev.* **1990**, *B41*, 7892.
(24) Vosko, S. H.; Wilk, L.; Nussair, M. *Can. J. Phys.* **1980**, *58*, 1200.
(25) Kawai, R.; Weare, J. H. *Phys. Rev. Lett.* **1989**, *65*, 80.
(26) Bylaska, E. B.; Taylor, P. R.; Kawai, R.; Weare, J. H. *J. Phys. Chem.* **1996**, *100*, 6966.
(27) Delley, B.; Freeman, A. J.; Ellis, D. E. *Phys. Rev. Lett.* **1983**, *50*, 488.
(28) Cheng, H.; Wang, L. *Phys. Rev. Lett.* **1996**, *77*, 51.
(29) Dhar, S.; Kestner, N. R. *Phys. Rev.* **1988**, *A38*, 1111.
(30) Lian, L.; Su, C. X.; Armentrout, *J. Chem. Phys.* **1992**, *97*, 4072.
(31) Moskovits, M.; DiLella, D. P.; Limm, W. *J. Chem. Phys.* **1984**, *80*, 626.
(32) Sung, M.; Kawai, R.; Weare, J. H. *Phys. Rev. Lett.* **1994**, *73*, 3552.
(33) Cheng, H. *J. Phys. Chem*. **1998**, *A102*.
(34) Goedecker, S.; Teter, M.; Hutter, J. *Phys. Rev.* **1996**, *B54*, 1703.
(35) Ramer, J. N.; Rappe, A. M. *Phys. Rev.* **1999**, *B59*, 12471.